ELSEVIER

Chemical Physics 266 (2001) 137–147

Chemical Physics

www.elsevier.nl/locate/chemphys

Hydrogen-bond lifetime measured by time-resolved 2D-IR spectroscopy: *N*-methylacetamide in methanol

S. Woutersen [a], Y. Mu [b], G. Stock [b], P. Hamm [a,*]

[a] *Max Born Institut für nichtlineare Optik und Kurzzeitspektroskopie, D-12489 Berlin, Germany*

[b] *Institut für Physikalische und Theoretische Chemie, J.W. Goethe Universität, Marie-Curie-Strasse 11, D-60439 Frankfurt, Germany*

Received 14 August 2000

Abstract

2D vibrational spectroscopy is applied to investigate the equilibrium dynamics of hydrogen bonding of *N*-methylacetamide (NMA) dissolved in methanol-d_4. For this particular solute–solvent system, roughly equal populations are found for two conformers of the solute–solvent complex, one of which forms a hydrogen bond from the C=O group of NMA to the surrounding solvent, and one of which does not. Using time-resolved 2D-IR spectroscopy on the amide I band of NMA, the exchange between both conformers is resolved. Equilibration of each conformer is completed after 4.5 ps, while the formation and breaking of the hydrogen bond occurs on a slower, 10–15 ps time scale. This interpretation is supported by classical molecular-dynamics simulations of NMA in methanol. The calculations predict a 64% population of the hydrogen-bonded conformer and an average hydrogen-bond lifetime of ≈12 ps.

1. Introduction

Solution phase dynamics critically influences the properties of molecules and their chemical reactivity. It is known from solvation experiments, using optical chromophores as a sensor, that most common solvents equilibrate on a very fast (sub-picosecond) time scale [1–6]. However, as solvation is thought to be driven by long-range Coulomb interaction, these measurements miss the details of the solute–solvent interaction. In particular when hydrogen bonding between solute and solvent occurs, the local structures around the solute might be quite long lived, much longer than the equilibration time of the bulk solvent [7–9]. As vibrational transitions are likely to be mostly sensitive to local interactions (i.e., anharmonic coupling), IR spectroscopy appears to be more appropriate to investigate local structures. As model system for such studies, we have chosen *N*-methylacetamide (NMA: CH_3–CONH–CH_3) dissolved in methanol. NMA is a commonly used model compound for the peptide (–CONH–) unit, and has been the subject of extensive experimental (see, e.g., Refs. [10–12]) and theoretical (see, e.g., Refs. [13–19]) investigations. It is well established that the frequency position of the so-called amide I band (mostly the C=O stretching mode) of NMA is an extremely sensitive measure for the strength of hydrogen bonds between the molecule and its surroundings. The absorption spectrum of NMA

* Corresponding author. Tel.: +49-30-6392-1410; fax: +49-30-6392-1429.

E-mail address: hamm@mbi-berlin.de (P. Hamm).

0301-0104/01/$ - see front matter
PII: S0301-0104(01)00224-5

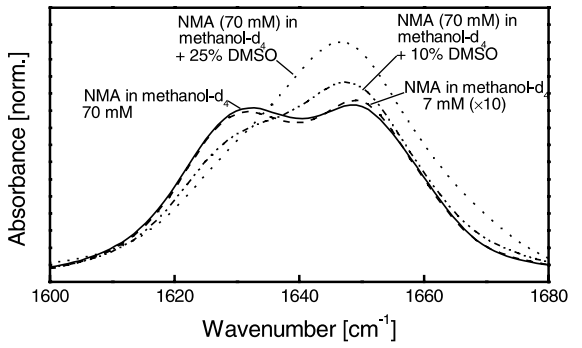

Fig. 1. Absorption spectrum of NMA in methanol-d_4 at a concentration of 70 mM (—) and 7 mM (- - -), and with 10% (vol.) DMSO ((·····) 70 mM) and 25% (vol.) DMSO added ((···) 70 mM). The 7 mM data are scaled accordingly.

in methanol in the spectral region of the amide I band shows a pronounced double peak structure (see Fig. 1), which, as we shall see, originates from a heterogeneous distribution of hydrogen-bond conformers of NMA–methanol complexes. The amide I band of NMA in methanol thus appears to be an ideal candidate to study hydrogen-bond dynamics. Hydrogen-bond dissociation and association reactions have been studied before [20–23], applying spectroscopy on the OH-stretching mode directly.

In a series of recent papers, the capability of 2D-IR spectroscopy for unraveling couplings between amide I states in small polypeptides has been demonstrated [24–26]. The 2D-IR spectroscopy applied in these studies is a quasi-frequency domain technique (double-resonance experiment) which measures the response of the sample as a function of probe frequency and the center frequency of a spectrally selective (10 cm^{-1}) pump pulse (which therefore is relatively long, see Section 2). It has been shown that electrostatic Coulomb interaction dominates the coupling [27,28], so that the couplings can be related to the three-dimensional structure of the peptide backbone [25]. With the help of polarization dependent 2D-IR spectroscopy, we recently succeeded to determine the backbone structure of a small peptide, trialanine, in water [26].

Here, we shall stress a second important aspect of 2D-IR spectroscopy, namely its potential of an ultrafast time resolution (in the order of 1 ps), which is perfectly suited to study fast solution phase processes. As a first step in this direction, we focus here on the hydrogen-bond formation and breaking dynamics of the 'peptide monomer' NMA. This was achieved by an extension of the methodology applied in Refs. [24–26], namely by additionally varying the time separation between pump and probe pulse. This technique might be viewed as the vibrational analogue of exchange spectroscopy known from NMR [29]. The difference, however, is the time scale of the particular exchange process studied here, which is orders of magnitudes faster than what would be accessible by NMR spectroscopy. To support the interpretation of experimental data, we have furthermore performed classical molecular-dynamics simulations of NMA in methanol. The calculations are found to be in full agreement with experiment and allow for a microscopic picture of the solvation dynamics.

2. Materials and methods

The output of a Spectra Physics Spitfire Ti:S laser/amplifier system (pulse duration: 80 fs, wavelength: 800 nm, repetition rate: 1 kHz) is used to generate intense mid-IR pulses in the 6 μm spectral range in a two step frequency conversion process. The signal and idler beam from a double stage BBO-optical parametrical amplifier ($d = 4$ mm, type II phase matching), seeded from a single filament white light, is difference frequency mixed in a $AgGaS_2$ crystal ($d = 1.5$ mm, type I phase matching). Tunable pulses with a typical pulse duration of 120 fs, spectral width of 160 cm^{-1}, and energy of 1 μJ are obtained routinely. Important for the present investigations is the remarkable energy stability of the setup (fluctuation of the spectral intensity <0.2–0.5% rms), which is smaller than that of the Ti:S amplifier system. The underlying noise-suppressing mechanism is discussed in detail elsewhere [30].

Probe frequency resolution is achieved by dispersing the probe pulses after passing the sample with the help of an imaging spectrograph ($f = 190$ mm, grating: 100 l mm^{-1}) and recording them with a 16 element MCT array detector. The detector

covers a spectral range of ≈100 cm^{-1} with a resolution of 6 cm^{-1}. Narrow band pump pulses are obtained by filtering the original pulses with the help of a tunable Fabry–Perot filter. It is constructed from two dielectric partial reflectors with $R = 90\%$, one of which being mounted on a piezo-controlled mirror mount. For the experiments shown in this paper, the Fabry–Perot has been aligned to seventh order of interference, yielding pulses with a spectral width of $\Delta\omega \approx 10$ cm^{-1} and a single-sided exponential temporal shape, whose fast rising edge is given by the pulse duration of the original IR pulses and the slope of which decays with $\tau = 700$ fs. The time–bandwidth product $\Delta\omega\tau = 0.20$ is close to the theoretical limit for a single-sided exponential pulse $\Delta\omega\tau = 1/2\pi$. The peak transmittance through the Fabry–Perot filter is ≈60% so that ≈40 nJ remain after filtering. The spectrum transmitted trough the Fabry–Perot filter is adjusted to the desired frequency position with the help of a computer controlled feedback loop. This is done between subsequent delay time scans by directing the pump beam instead of the probe beam onto the entrance slit of the spectrometer with the help of an automatic shutter. Drifts of the Fabry–Perot filter during individual scans are negligible.

Stray light from the pump beam and mechanical vibrations from the light chopper cause a small delay independent background (in the order 0.1 mOD) which is measured independently at a delay time position of −5 ps, when no transient response from the sample is present, and subtracted from the data. The averaging time is continuously increased as the signal size decreases as a function of pump–probe delay time. The noise level of each individual data point was estimated from the statistics of the individual measurements. The data in Fig. 2b have a noise level of $\approx 4 \times 10^{-6}$ OD (rms) which is reached after ≈3 min averaging time per 16 data points. The anisotropy experiments are performed by rotating the pump polarization by 90° with the help of a zero-order half-wave plate and maintaining all other lasers parameters unchanged.

N-methylacetamide, deuterated methanol, and DMSO were obtained from Aldrich and used without further purification. Complete exchange of the proton amide proton was monitored by the shift of the amide II band. The time-resolved data were measured at a concentration of 70 mM in a CaF_2 cell with 50 μm spacing. Excitation densities were below 1%. All experiments were performed at room temperature (20°C).

The molecular-dynamics simulations were performed with the GROMOS96 simulation program package employing the GROMOS force field 43A1 [31]. NMA was placed in a periodic truncated

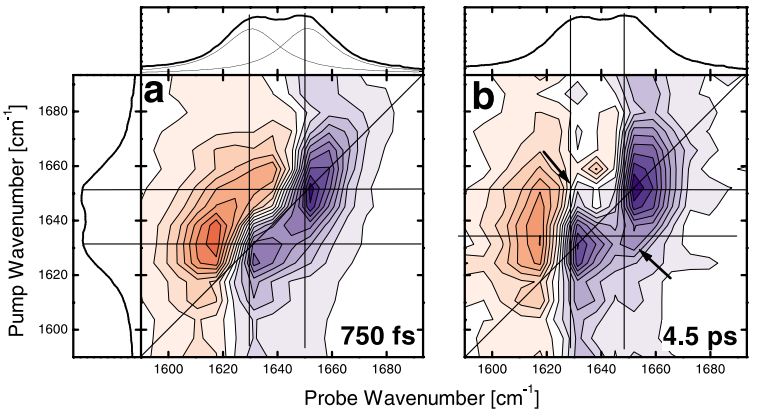

Fig. 2. 2D-IR spectrum of NMA in methanol-d_4 with the delay between pump and probe pulse varied from 750 fs to 4.5 ps. Vibrational T_1-relaxation, which diminishes the total signal size, is normalized out. The contour lines represent a linear scale from −1.2 to +1.2 mOD in (a) and −0.1 to +0.1 mOD in (b). Blue colors mark signal with negative transient response (bleach and stimulated emission), while red colors mark positive signals (excited state absorption).

octahedral with 286 methanol molecules. The equation of motion was integrated by using a leapfrog algorithm with a time step of 2 fs. Covalent bond lengths were constrained with the procedure SHAKE [32] with a relative geometric tolerance of 0.0001. A twin-range cutoff of 8/14 Å was used for the nonbonded interactions, and a reaction-field correction with permittivity $\varepsilon_{RF} = 18$ was employed. The solute and methanol were separately weakly coupled to a temperature bath of 293 K using a 0.1 ps coupling time [33]. The total system was also weakly coupled to a pressure bath of 1 atm using a 0.5 ps relaxation time. The equilibration protocol consisted of 50 steps of steepest-descent minimization applied to the solvent molecules with fixed solute, followed by a 5 ps molecular-dynamics simulation of the solvent with fixed NMA, and another 5 ps simulation without position constraining of the NMA molecule. The simulation was then continued for 9 ns at 293 K, whereby the coordinates were saved every 0.1 ps for analysis.

3. Experimental results

Fig. 1 shows the absorption spectrum of NMA in methanol-d_4 (CD_3OD) in the spectral range of the amide I band (at room temperature). A small background from the solvent, originating from either an overtone or a combination mode, but not from a fundamental mode of methanol-d_4, has been subtracted in Fig. 1. The most striking feature is a pronounced double peak structure which can be satisfactorily fit by two Lorentzian lines with peak positions of 1631 and 1651 cm^{-1} and almost identical widths (25 cm^{-1} FWHM) and intensities. [1] The double peak structure does not vanish with lowered concentration (solid line: 70 mM, dashed line: 7 mM, scaled accordingly) but changes the equilibrium between both states slightly. Adding 10% (vol.) of DMSO (dashed-dotted line), on the other hand, significantly shifts the equilibrium towards the high frequency peak, while only the high frequency peak remains for 25% (vol.) DMSO (dotted line).

Fig. 2 shows the time-resolved 2D-IR spectrum of NMA in methanol-d_4 (concentration 70 mM) for parallel polarizations of the pump and probe beams. The time-resolved 2D-IR spectrum measures the response of the sample as a function of probe frequency, the center frequency of a relatively narrow band pump pulse (see Section 2) and the delay time between the pump and probe pulses. [2] The early 2D-IR spectrum measured at 750 fs (when the temporal overlap between pump and probe pulse is negligible) features for each of both states a bleach and stimulated emission signal along the diagonal of the graph (negative absorption change, marked in blue) together with the anharmonically redshifted $v = 1 \rightarrow v = 2$ excited state absorption, in agreement with the previously determined anharmonicity of $\approx$16 cm^{-1} [24] (positive absorption change, marked in red). The double peak structure of the absorption spectrum is also evident in the 2D-IR spectrum. The individual 2D peaks are elongated along the diagonal of the 2D spectrum. Each bleach-excited-state-absorption pattern will be called diagonal peak in the following.

Fig. 3 shows a cut through the early 2D-IR spectrum for pump frequencies resonant with either of the peaks of the NMA absorption spectrum (1631 and 1652 cm^{-1}, respectively). In both cases, a negative bleach and stimulated emission signal is observed together with the anharmonically shifted excited state absorption, without any evidence for coupling between both bands, as it was observed for connected peptide units in small polypeptides [25,26]. Furthermore, the results for parallel (solid lines) and perpendicular polarizations (dotted lines) of pump and probe are essentially indistin-

[1] As we shall see from the time-resolved 2D-IR spectroscopy, the line shape is neither a Lorentzian, Gaussian nor a Voigt profile, but includes rather complicated dynamics. The fit of the linear absorption spectrum with Lorentzian functions is therefore certainly unphysical and is meant only to label both peaks with their peak frequency.

[2] Delay time zero is defined by the maximum of the asymmetric cross-correlation function which has the shape of a single-sided exponential (the output from the Fabry–Perot filter, see Section 2).

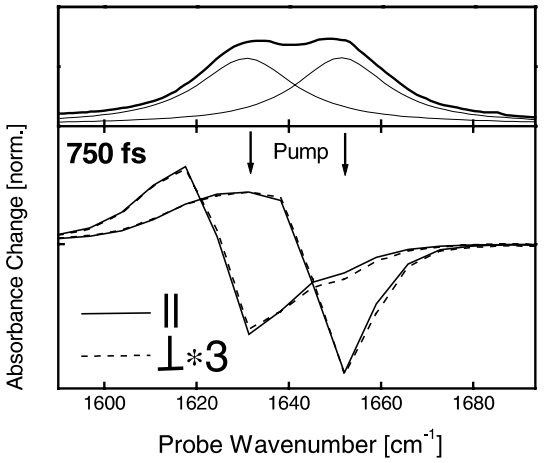

Fig. 3. Cuts through the 750 fs 2D-IR spectrum for two pump frequencies (1631 and 1652 cm^{-1}) resonant with either of the two absorption peaks of NMA in methanol-d_4. The transient responses with parallel (—) and perpendicular ((- - -) scaled by a factor 3) polarization of pump and probe pulses are compared.

guishable after multiplication of the latter by a factor 3.

With increasing delay time between the pump and probe pulses, the 2D response changes significantly. The most prominent effect is an overall decay of the signal due to T_1-relaxation into the vibrational ground state. This decay is depicted in Fig. 4b for pump and probe frequencies resonant with either of the absorption bands (i.e., $\omega_{\text{pump}} = 1652\ cm^{-1}$, $\omega_{\text{probe}} = 1652\ cm^{-1}$ and $\omega_{\text{pump}} = 1631\ cm^{-1}$, $\omega_{\text{probe}} = 1631\ cm^{-1}$). Both transitions decay almost equally fast, with time constants of $T_1 = 1.6 \pm 0.3$ and 2.0 ± 0.3 ps for the 1652 and 1631 cm^{-1} band, respectively. T_1-relaxation is normalized out in Figs. 2 and 4a in order to facilitate comparison of the shape of the 2D spectra. Two phenomena are to be distinguished: (a) The diagonal peaks, which are elongated along the diagonal in the early 2D-IR spectrum, are orientated parallel to pump frequency axis in the late 4.5 ps spectrum. (b) With increasing delay, additional sub-structure emerges in the cross-peak regions ($\omega_{\text{pu}} = 1631\ cm^{-1}$, $\omega_{\text{pr}} = 1651\ cm^{-1}$ and $\omega_{\text{pu}} = 1651\ cm^{-1}$, $\omega_{\text{pr}} = 1631\ cm^{-1}$, see arrows in Fig. 2). The temporal evolution of the signal is depicted in Fig. 4a, which shows cuts through the time-resolved 2D spectra for one fixed pump frequency chosen to be resonant with the 1651 cm^{-1} band. After a time of ≈2 ps, a cross-peak emerges in the spectral region of the 1631 cm^{-1} band. Just like the diagonal peak, the cross-peak consists of a

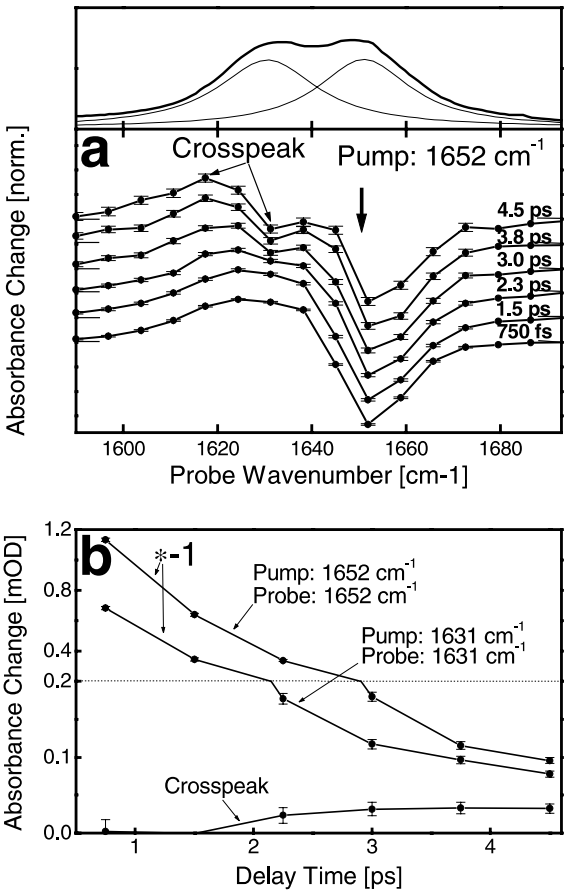

Fig. 4. (a) Cuts through the time-resolved 2D-IR spectra for a fixed pump frequency (1652 cm^{-1}) chosen to be resonant with one of the absorption peaks. After a delay time of ≈2 ps, a cross-peak emerges, which reflects population transfer between both sub-states. (b) Decay of both diagonal peaks due to vibrational T_1-relaxation compared with the rise of the cross-peak. The absorption change axis scaling is stretched for values smaller than 0.2 mOD to facilitate comparison of the relatively small cross-peak intensity. The bleach signal is plotted for the diagonal peaks (multiplied by −1), while half the difference between the negative and positive dip is plotted for the off-diagonal peak, as indicated in (a). This procedure largely suppresses the background from the dominating excited state absorption of the diagonal band. The small background, which still remains, is subtracted to obtain zero cross-peak intensity at delay time zero. Error bars indicate $\pm 1\sigma$.

negative bleach contribution (around 1630 cm^{-1}) and an anharmonically shifted excited state absorption (around 1615 cm^{-1}). The cross-peak exhibits significant spectral overlap with the $v = 1 \rightarrow v = 2$ excited stated absorption of the $\omega_{pu} = 1651\ cm^{-1} - \omega_{pr} = 1651\ cm^{-1}$ diagonal peak so that it sits on a positive background.

Fig. 4b compares the cross-peak intensity with that of the corresponding diagonal peaks. In order to obtain a measure which approximately resembles the populations in the corresponding states, the pure bleach signal is plotted for the diagonal peaks (with inverted sign), while half the difference between the negative and positive dip is plotted for the off-diagonal peak (as indicated in Fig. 4a). This procedure yields a measure for the off-diagonal intensity, which largely suppresses the background from the dominating excited state absorption of the corresponding diagonal band. The small background, which still remains, is subtracted to obtain zero cross-peak intensity at early delay times. That the cross-peak intensity is indeed zero at early delay times is concluded from the equivalence of the parallel and perpendicular 2D-IR spectrum (see Section 4). As already discussed before, the diagonal-peak intensities decay exponentially as function of time, reflecting vibrational relaxation of the amide I states. The cross-peak intensity, on the other hand, initially increases and then slowly approaches that of the diagonal peaks.

4. Discussion

The amide I band of NMA has been extensively studied by FTIR and (resonance) Raman spectroscopy, and the frequently observed substructure has been attributed to two effects: (a) dimerization or polymerization [12] and (b) resonance coupling between the amide I mode and OH-bending modes of solvent molecules (e.g. water) which are hydrogen bonded to the NMA molecules [10]. The latter effect can be excluded in the present case since deuteration separates the OD resonance of methanol-d_4 from that of the amide I band of NMA. Dimerization of NMA, on the other hand, has been studied in detail in different solvents [12]. The concentration, at which dimerization begins to be significant, strongly depends on the ability of the solvent to form hydrogen bonds with NMA molecules and separating them from each other. This concentration varies from 6 M in water to 100 mM in acetonitrile [12]. Since the hydrogen-bond capability of methanol lies in-between both examples, it is concluded that dimerization cannot play a role in the range of concentrations considered here 7–70 mM [34] and thus cannot be responsible for the double peak structure in the spectrum.

Besides these conventional arguments, 2D-IR spectroscopy provides additional, and completely novel tools to study the origin of such sub-structure in vibrational bands. If dimerization of two NMA molecules were the reason for the splitting, a pronounced coupling between both amide I states would be observed, manifesting itself as cross-peaks in the early, or instantaneous, 2D-IR spectrum. These cross-peaks have been extensively discussed for coupled amide I modes in polypeptides [24–26], but cannot be identified for NMA in methanol-d_4. Furthermore, under the assumption of degeneracy (which would be the case for a homo-dimer of two chemically identical molecules) both excitonic states would have perpendicular transition dipole moments. In this case, the coupled excitonic eigenstates would be the symmetric and anti-symmetric linear combination $1/\sqrt{2}(|1\rangle \pm |2\rangle)$ of the zero-order states $|1\rangle$ and $|2\rangle$. Their transition dipole vectors are perpendicular (since $1/2(\vec{\mu}_1 + \vec{\mu}_2) * (\vec{\mu}_1 - \vec{\mu}_2) = 1/2(|\vec{\mu}_1|^2 - |\vec{\mu}_2|^2) = 0$) for a homo-dimer (for which the absolute squares of the transition dipoles $|\vec{\mu}_1|^2$ and $|\vec{\mu}_2|^2$ are identical), regardless on the relative orientation $\vec{\mu}_1\vec{\mu}_2$. As a consequence, the cross-peak would be much more pronounced in the 2D spectrum measured with perpendicular polarization of the pump and probe pulses [25,26]. Even for the nondegenerate case, the cross-peak anisotropy would still be less than 0.4 so that a polarization dependence of the ratio of the cross- and diagonal-peak intensities is to be expected. In contrast, the transient response measured with perpendicular polarization, multiplied by a factor 3, perfectly resembles that of parallel polarization (see Fig. 3). The factor 3, which corresponds to an anisotropy of $r = 0.4$ or an angle of $\varphi = 0°$ ($r = 1/5(3\cos^2\varphi - 1)$), is the

expected ratio when pumped and probed transition are parallel, or, as in this case, identical. Similar arguments would hold when resonance coupling to solvent modes [10] or a Fermi resonance [35] would be the origin of the double peak structure. We therefore conclude that it is indeed a heterogeneous ensemble of NMA monomers, which gives rise to the absorption spectrum. The double peak structure is thus to be explained by an equilibrium between two configurations of the solute–solvent system. It is well established that the amide I absorption frequency is significantly redshifted by hydrogen bonding [10,11,13,14]. DMSO is a solvent with roughly equal polarity as methanol, which however is aprotic and thus cannot form hydrogen bonds with the C=O group of NMA. Adding small amounts of DMSO (10%) significantly shifts the equilibrium between both NMA sub-states towards the higher frequency state. Apparently, the amount of DMSO added efficiently saturates the –OD sites of methanol so that more NMA molecules remain unbound at the C=O site. We therefore conclude that the double peak structure reflects an equilibrium of NMA molecules which are either hydrogen bonded or essentially isolated at the C=O group. This assignment is supported by the separation of both peaks ($\approx$20 cm^{-1}), which perfectly matches the prediction from ab initio calculations for the effect of a hydrogen bond at the C=O site [14]. A shift of the same order is also observed when comparing the amide I frequency of NMA dissolved in aprotic (such as DMSO) and protic solvents (e.g. water). The effect on the NH group, on the other hand, has been shown to be considerably smaller [14]. The equilibrium constant between both configurations happens to be close to unity for this particular solvent–solute system, rendering it an ideal candidate to study its exchange dynamics.

We are now in a position to discuss the time dependence of the transient response: The T_1-relaxation of amide I modes has been found to be fast, with time constants in the order of 1–2 ps. The relaxation rate does essentially not depend on the particular molecule [24], the temperature [36], or, as shown here, the solvent and it was concluded that it reflects an intrinsic property of the peptide unit rather than an effect of the surrounding [24]. The present result is yet another verification of this conclusion. In particular, the T_1-relaxation rate is not significantly affected by hydrogen-bond configuration of the NMA molecule. The pathway of the energy flow, however, remains an open question and will be addressed elsewhere.

Here, we shall focus on the temporal evolution of the remaining signal, which is attributed to those molecules which have not yet decayed and are still in the vibrational excited state. Since the energy pumped into the system is relatively small ($\approx$1600–1700 cm^{-1}), one may assume that vibrational excitation does not significantly perturb the motion of molecule, and merely serves as a label. This is in particular true for those molecules, to which this technique is sensitive, namely those which are still in the excited state so that the pump energy is not yet dissipated into low frequency modes or the bath. In other words, the equilibrium fluctuations of the peptide in its solvent surrounding can be followed within a time window limited by the lifetime of the label, which is the vibrational excitation lifetime T_1.

In the early 2D-IR spectrum, the diagonal peaks are elongated and orientated parallel to the diagonal. The response of the sample follows of the pump pulse frequency, or, in other words, the pump pulse burns holes into absorption spectrum, the width of which being narrower than that of the absorption spectrum. Consequently, the absorption spectrum is to some extent inhomogeneously broadened at each instant of time. However, solution phase systems are highly flexible and inhomogeneity is a question of time scales. Since all solvent molecules are chemically identical, all inhomogeneity must vanish after some sufficiently large time. This time corresponds to the lifetime of local structures of the solvent–solute complexes. The narrow band pump pulse labels a certain subensemble of molecules, namely those which happen to be resonant with the pump pulse. As the absorption frequency is in some way affected by the local surrounding of the molecule, the pump pulse labels a certain sub-ensemble of local structures. If the system were static, the spectroscopic response would also be static, in contrast to the experimental result. Due to the equilibrium fluctuations of the system, the initial heterogeneity

equilibrates until all memory about the initial configuration is lost. After that time, the system appears to be homogeneously broadened and the spectroscopic response no longer depends on pump frequency.

At this point, we have to distinguish two phenomena: equilibration within individual sub-states, and equilibration between them. The former process leads to a broadening of the individual 2D bands together with a rotation of their orientation from diagonal at early times (inhomogeneously broadened) towards parallel to the pump frequency axis (homogeneously broadened). This process is evident from the experimental data (see Fig. 2) and appears to be essentially completed after 4.5 ps. A detailed analysis yields a time scale of ca. 2 ps for this spectral diffusion process. The appearance of a cross-peak, on the other hand, represents equilibration between both sub-states. With a certain probability, some of the initially excited molecules (e.g. those which are not hydrogen-bonded initially as in Fig. 4a), hop to the other configuration, i.e., form or break a hydrogen bond. In other words, cross-peaks emerge, which reflect population transfer between both sub-states. Vibrational excitation of the amide I mode, which merely serves as a label, is not affected by the hopping between both sub-states, so that these cross-peaks exhibit the same shape as would be obtained when exciting the coupled state directly. In other words, the cross-peaks exhibit the same bleach-excited-state-absorption pattern as the diagonal peaks. Similar conclusions were drawn from picosecond time-resolved double resonance experiments on the hydrogen-bond dynamics of Et_3SiOH in acetonitrile [23]. It is important to distinguish between the physical origin of the cross-peaks discussed here, which reflects a population interconversion process and hence is an incoherent phenomenon, and the cross-peaks observed in polypeptides [24–26], which is a coherent (i.e., excitonic) coupling process.

Interestingly, the distribution within each sub-state equilibrates entirely in 4.5 ps, as deduced from the homogeneous 2D line shape of the individual diagonal peaks. Equilibration between the sub-states, on the other hand, is still incomplete after that time. This can be concluded from the relatively small amplitude of the cross-peaks as compared to the diagonal peaks. After complete equilibration, both states would be equally populated so that diagonal and cross-peak should have approximately equal intensity, which clearly is not yet the case at 4.5 ps. The intensity ratios show that at 4.5 ps the population in the initially excited sub-state is still three times larger than in the other sub-state, so that equilibration between both sub-states is estimated to take place on a 10–15 ps time scale. This time reflects the lifetime of hydrogen bonds between NMA and surrounding methanol molecules and compares well with the typical time scales for hydrogen-bond dissociation and association observed for other molecular systems [21–23].

To support these ideas by a theoretical analysis, we have performed molecular-dynamics simulations of NMA in methanol. While a full account of this work will be given elsewhere [37], here we focus on the simulation results on the formation and breaking of intermolecular hydrogen bonds. As an indicator for these dynamics, we have considered the distance d_{OH} between the oxygen atom of NMA and the hydrogen atom of the OH group of methanol. Fig. 5 shows the typical time evolution of this quantity monitored for the three methanol molecules that are closest to the oxygen atom of NMA. Interestingly, the system shows a clear two-state behavior: Either there is a hydrogen bond, which is characterized by an average distance $\bar{d}_{OH} \approx 1.9$ Å and small (≈ 0.2 Å) root-mean-square fluctuations, or there is no hydrogen bond, which is accompanied by large fluctuations with a typical average distance of $\bar{d}_{OH} \approx 4$ Å. These fluctuations are mainly due to the fact that in the nonbonded case the three nearest methanol molecules are frequently exchanged, i.e., a methanol molecule that is first close to NMA may move away and is then replaced by another solvent molecule. In the case of a hydrogen bond, on the other hand, the methanol molecule participating in the bond remains the same during the lasting time of this bond, thus resulting in a comparatively stable state of the system. Furthermore, it is found that usually only a single hydrogen bond can be formed between the C=O group of NMA and methanol. However, there may be an additional

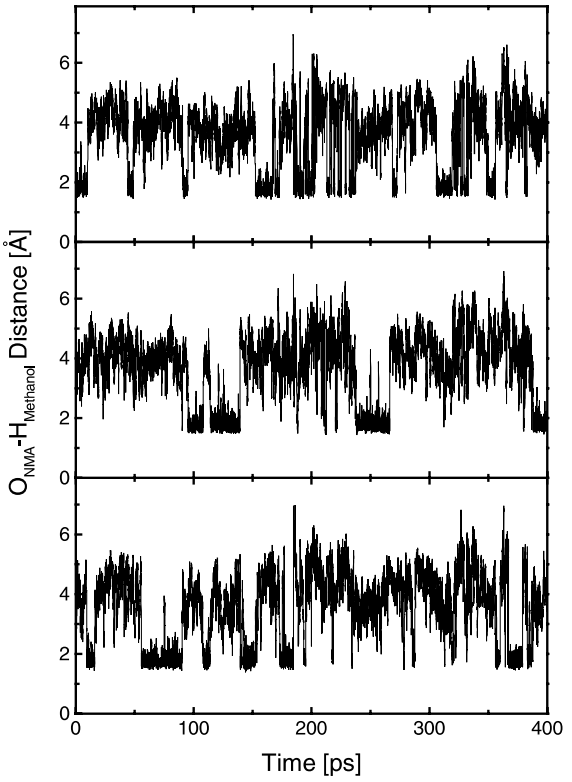

Fig. 5. Time evolution of the distances between the oxygen atom of NMA and the hydrogen atoms of the three nearest methanol molecules.

hydrogen bond between the oxygen atom of methanol and the hydrogen atoms of NMA [37].

In order to calculate the average lifetime of a hydrogen bond, we employ the GROMOS criterion that requests a maximum proton–acceptor distance of 2.5 Å and a minimum donor–proton–acceptor angle of 125° [31]. Fig. 5 clearly reconfirms that the first requirement is an appropriate condition to define a hydrogen bond. To exclude rapid large-amplitude fluctuations, moreover, the analysis of the data in Fig. 5 suggests to require a minimum bond lasting time of 2 ps (see also the discussion in Ref. [38]). That is, hydrogen bonds that are broken and reformed between the same partners within 2 ps are counted as a single continuous bond, while bonds lasting shorter than 2 ps are not included in the life time analysis. Proceeding this way, we counted a total of 488 hydrogen-bond events during the 9 ns simulation. The total lasting time of these bonds was 5.74 ns, which corresponds to a 64% population of the hydrogen-bonded conformer and to an average hydrogen-bond lifetime of 11.7 ps. The calculated relative population of 64% agrees well with the equilibrium constant of approximately unity derived from the linear absorption spectrum, and the calculated hydrogen-bond lifetime is very close to the value of 10–15 ps found from the time-resolved 2D experiments.

A simplified picture of the dynamics is shown in Fig. 6. The system quickly samples all configurations within one of the local minima of the free energy surface, until it occasionally hops to the other one. This behavior represents a very elementary example of the concept of a 'rugged energy landscape' which is commonly used to explain solution, glass and protein dynamics [39–41]. In particular protein dynamics is determined by an extended hierarchy of time scales, which start from such fundamental processes like the formation and breaking of local hydrogen bonds (1–10 ps) and ends at conformational dynamics of the quarternary protein structure (1 ms–1 s). For each level in this hierarchy, schemes similar to Fig. 5 are commonly applied. Even though the dynamics within each hierarchy level is much slower than that of the lower level, it is actually the sampling rate in the latter which determines the rate of the former. This is why a complete understanding of the complexity of protein dynamics requires spectroscopic tools which allow to access all levels in the

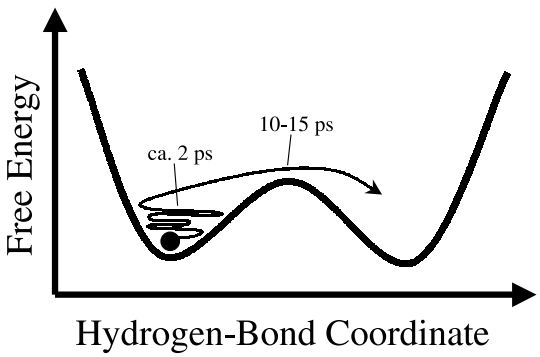

Fig. 6. Schematics explaining the observed dynamics. The system quickly samples all configurations within each of the local minima of the free energy surface, until it occasionally hops to another one.

hierarchy. 2D-IR spectroscopy appears to be particularly suited to study the very fundamental, but also extremely fast processes, for which other established spectroscopic techniques lack sufficient time resolution.

5. Conclusion

Each pump-frequency slice through the 2D spectra can be viewed as a conventional transient hole-burning experiment, used in previous studies to investigate e.g. H-bond dynamics [21–23]. Nevertheless, representing the vibrational response as 2D-contour plots provides a novel means to distinguish between homogeneous broadening, inhomogeneous broadening and spectral diffusion processes by simple inspection of the 2D line shapes. A nice theoretical discussion of 2D line shapes and their information content has been published recently [42].

Another potential of 2D spectroscopy shall be briefly addressed here. It is a common problem in vibrational spectroscopy that lines split into substructure and it is generally not straightforward to identify the splitting mechanisms (e.g. dimerization or polymerization, heterogeneous distribution of conformations, Fermi resonances, anharmonic couplings etc.). The peculiarities of the amide I band of NMA in water constitute a prominent example of this problem [10,12]. 2D-IR spectroscopy, and in particular polarization dependent 2D-IR spectroscopy (Fig. 3), can unambiguously reveal whether both transitions share a common energy level and hence helps significantly to resolve the origin of such splittings.

The spectroscopy described here might be viewed as the vibrational analogue of the exchange effect known from NMR spectroscopy. However, due to exchange narrowing, the exchange process studied here would be observed as a purely homogeneous phenomenon in NMR spectroscopy. The crucial difference is the time scale of the IR measurement process, which is several orders of magnitude faster. Moreover, as demonstrated here, the timescale accessible by 2D-IR methods is the same as that which within reach of MD simulations, making possible a direct link between real and computer experiment. Since much of the fundamental dynamics of solution phase systems happen on this fast picosecond time scale, important new insight are to be expected from time-resolved 2D-IR spectroscopy.

Acknowledgements

We thank Reinhard Schweitzer-Stenner, Erik Nibbering and Wilfred van Gunsteren for valuable discussions and Thomas Elsaesser for critically reading the manuscript and continuous support of the project. One of us (YM) gratefully acknowledges the Alexander Humboldt foundation for a visiting scientist fellowship. This work was supported by the Deutsche Forschungsgemeinschaft.

References

[1] M.L. Horng, J.A. Gardecki, A. Papazyan, M. Maroncelli, J. Phys. Chem. 99 (1995) 17311.
[2] G.R. Fleming, M. Cho, Annu. Rev. Phys. Chem. 47 (1996) 109.
[3] R. Jimenez, G.R. Fleming, P.V. Kumar, M. Maroncelli, Nature 369 (1994) 471.
[4] M. Cho, J.-Y. Yu, T. Joo, Y. Nagasawa, S.A. Passino, G.R. Fleming, J. Phys. Chem. 100 (1996) 11944.
[5] P. Vöhringer, D.C. Arnett, R.A. Westervelt, M.J. Feldstein, N.F. Scherer, J. Chem. Phys. 102 (1995) 4027.
[6] S.A. Kovalenko, J. Ruthman, N.P. Ernsting, J. Chem. Phys. 109 (1998) 1894.
[7] P. Hamm, M. Lim, R.M. Hochstrasser, Phys. Rev. Lett. 81 (1998) 5326.
[8] C. Chudoba, E.T.J. Nibbering, T. Elsaesser, Phys. Rev. Lett. 81 (1998) 3010.
[9] C. Chudoba, E.T.J. Nibbering, T. Elsaesser, J. Phys. Chem. A 103 (1999) 5625.
[10] X.G. Chen, R. Schweitzer-Stenner, S. Krimm, N.G. Mirkin, S.A. Asher, J. Am. Chem. Soc. 116 (1994) 11141.
[11] X.G. Chen, R. Schweitzer-Stenner, S.A. Asher, N.G. Mirkin, S. Krimm, J. Phys. Chem. 99 (1995) 3074.
[12] R. Schweitzer-Stenner, G. Sieler, H. Christiansen, Asian J. Phys. 7 (1998) 287.
[13] N.G. Mirkin, S. Krimm, J. Mol. Struct. 377 (1996) 219.
[14] H. Torii, T. Tatsumi, M. Tasumi, Mikrochim. Acta 14 (1997) 531.
[15] W.L. Jorgensen, J. Phys. Chem. 90 (1986) 1276.
[16] H. Guo, M. Karplus, J. Phys. Chem. 96 (1992) 7273.
[17] Y. Ding, D.N. Bernardo, K. Krogh-Jespersen, R.M. Levy, J. Phys. Chem. 99 (1995) 11575.

[18] W.-G. Han, S. Suhai, J. Phys. Chem. 100 (1996) 3942.
[19] J. Gao, M. Freindorf, J. Phys. Chem. A 101 (1997) 3182.
[20] H. Graener, T.Q. Ye, J. Phys. Chem. 93 (1989) 5963.
[21] H. Graener, T.Q. Ye, A. Laubereau, J. Chem. Phys. 90 (1989) 3413.
[22] G. Seifert, H. Graener, J. Phys. Chem. 98 (1994) 11827.
[23] S.M. Arrivo, E.J. Heilweil, J. Phys. Chem. 100 (1996) 11975.
[24] P. Hamm, M. Lim, R.M. Hochstrasser, J. Phys. Chem. B 102 (1998) 6123.
[25] P. Hamm, M. Lim, W.F. DeGrado, R.M. Hochstrasser, Proc. Natl. Acad. Sci. USA 96 (1999) 2036.
[26] S. Woutersen, P. Hamm, J. Phys. Chem B 204 (2000) 11316.
[27] S. Krimm, J. Bandekar, Adv. Protein Chem. 38 (1986) 181.
[28] H. Torii, M. Tasumi, J. Chem. Phys. 96 (1992) 3379.
[29] R.R. Ernst, G. Bodenhausen, A. Wokaun. Principles of Nuclear Magnetic Resonance in One and Two Dimensions, Oxford University Press, Oxford, 1987.
[30] P. Hamm, R.A. Kaindl, J. Stenger, Opt. Lett. 25 (2000) 1798.
[31] W.F. van Gunsteren, S.R. Billeter, A.A. Eising, P.H. Hünenberger, P. Krüger, A.E. Mark, W.R.P. Scott, I.G. Tironi, Biomolecular Simulation: The GROMOS96 Manual and User Guide, Vdf Hochschulverlag AG an der ETH Zürich, Zürich, 1996.
[32] J.-P. Ryckaert, G. Ciccotti, H.J.C. Berendsen, J. Comp. Phys. 23 (1977) 327.
[33] H.J.C. Berendsen, J.P.M. Postma, W.F. van Gunsteren, A. DiNola, J.R. Haak, J. Chem. Phys. 81 (1984) 3684.
[34] R. Schweitzer-Stenner, personal communication.
[35] In press.
[36] K.A. Peterson, C.W. Rella, J.R. Engholm, H.A. Schwettman, J. Phys. Chem. B 103 (1999) 557.
[37] Y. Mu, G. Stock, in press.
[38] A.M.J.J. Bonvin, M. Sunnerhagen, G. Otting, W.F. van Gunsteren, J. Mol. Biol. 282 (1998) 859.
[39] H. Frauenfelder, S.G. Sligar, P.G. Wolynes, Science 254 (1991) 1598.
[40] W.A. Eaton, P.A. Thompson, C.-K. Chan, S.J. Hagen, J. Hofrichter, Structure 4 (1996) 1133.
[41] P.G. Wolynes, Z. Luthey-Schulten, J.N. Onuchic, Chem. Biol. 3 (1996) 425.
[42] A. Tokmakoff, J. Phys. Chem. A 104 (2000) 4247.